JCTC Journal of Chemical Theory and Computation

Electronic Energy Transfer in Condensed Phase Studied by a Polarizable QM/MM Model

Carles Curutchet,*,† Aurora Muñoz-Losa,‡ Susanna Monti,§ Jacob Kongsted,|| Gregory D. Scholes,† and Benedetta Mennucci‡

Department of Chemistry, 80 St. George Street, Institute for Optical Sciences, and Centre for Quantum Information and Quantum Control, University of Toronto, Toronto, Ontario, M5S 3H6 Canada, Dipartimento di Chimica e Chimica Industriale, Università di Pisa, via Risorgimento 35, 56126 Pisa, Italy, Istituto per i Processi Chimico-Fisici (IPCF-CNR), Area della Ricerca, via G. Moruzzi 1, I-56124 Pisa, Italy, and Department of Physics and Chemistry, University of Southern Denmark, Campusvej 55, DK-5230 Odense M, Denmark

Received March 23, 2009

Abstract: We present a combined quantum mechanics and molecular mechanics (QM/MM) method to study electronic energy transfer (EET) in condensed phases. The method introduces a quantum mechanically based linear response (LR) scheme to describe both chromophore electronic excitations and electronic couplings, while the environment is described through a classical polarizable force field. Explicit treatment of the solvent electronic polarization is a key aspect of the model, as this allows account of solvent screening effects in the coupling. The method is tested on a model perylene diimide (PDI) dimer in water solution. We find an excellent agreement between the QM/MM method and "exact" supermolecule calculations in which the complete solute−solvent system is described at the QM level. In addition, the estimation of the electronic coupling is shown to be very sensitive to the quality of the parameters used to describe solvent polarization. Finally, we compare ensemble-averaged QM/MM results to the predictions of the PCM-LR method, which is based on a continuum dielectric description of the solvent. We find that both continuum and atomistic solvent models behave similarly in homogeneous media such as water. Our findings demonstrate the potential of the method to investigate the role of complex heterogeneous environments, e.g. proteins or nanostructured host materials, on EET.

1. Introduction

Electronic energy transfer (EET) is a fundamental nonradiative process involving de-excitation of a donor molecule and concomitant electronic excitation of a nearby acceptor.[1] EET is used to harvest light in photosynthesis with near-perfect efficiency[2−4] and is intrinsic to many applications in materials and life sciences. Some examples include the design of artificial light-harvesting antennae,[5−8] the optimization of organic light-emitting diodes,[9−12] and the measurement of distances in biological systems.[13−15]

Much progress related to EET was incubated more than 50 years ago, when Förster proposed an elegant theory relating experimental observables to the mechanisms of EET.[16] Despite the success of the Förster theory in explaining EET dynamics in a wide variety of systems, researchers have identified a number of situations in which such a theory can fail.[17] Non-Förster effects include the breakdown of the point dipole approximation used to describe the electronic coupling,[18−21] distance-dependent dielectric screening effects,[22,23] and the need to evaluate the spectral overlap factor from homogeneously broadened absorption and emission spectra and subsequently averaging over inhomogeneous, i.e.

* Corresponding author e-mail: ccurutch@chem.utoronto.ca.
† University of Toronto.
‡ Università di Pisa.
§ Istituto per i Processi Chimico-Fisici (IPCF-CNR).
|| University of Southern Denmark.

10.1021/ct9001366 CCC: $40.75
Published on Web 06/04/2009

static, disorder.[24−26] In addition, in multichromophoric aggregates it is necessary to account for effective donor/acceptor states shared over multiple strongly coupled chromophores.[26−28] Photosynthetic proteins represent a paradigmatic case in which such effects are significant. Moreover, recent experimental evidence points to the importance of wavelike coherent energy transfer in such systems, in contrast to the traditionally assumed Förster incoherent hopping mechanism, suggesting that the protein plays an active role in protecting electronic coherences between the electronic states of the pigments.[29,30] In this context, a combination of both elaborate experimental and theoretical approaches are needed in order to assess the significance of such non-Förster effects and, in particular, to gain fundamental insights into the role of the protein structure and dynamics on the overall process.

In the past decade, much theoretical effort has been directed toward the accurate prediction of electronic couplings from quantum mechanical (QM) methods, thus overcoming the point dipole approximation.[18−21,31,32] The accuracy of these approaches depends mainly on the quality of the QM level of theory and basis set adopted.[33] However, detailed theoretical insights on the role of solvation on EET have eluded researchers for a long time. Typically, the simple screening factor introduced by Förster, $1/n^2$, where n is the refractive index of the medium, is used. The significance of this factor is evident, as it can reduce the EET rate by a factor of $\sim$4 in typical environments.

A significant advance in the field has been the development of a QM method to study EET between molecules in condensed phase.[31,34] This method is based on a linear response (LR) approach (either within Hartree−Fock and density functional theory or semiempirical approaches) and introduces the effect of the environment in terms of the polarizable continuum model (PCM). In the PCM model,[35] the solvent is represented as a polarizable continuum medium characterized by its macroscopic dielectric properties, whereas the solute, located in a molecular-shaped cavity inside the dielectric, is described at a full QM level. Such a methodology allows for a consistent treatment of solvent effects on both the evaluation of the excited states and the electronic coupling and in addition properly accounts for molecular shape, thus overcoming a fundamental limitation of Förster's screening factor. By applying this method, we recently discovered that the molecular shape indeed has a strong influence on the screening of the electronic couplings between photosynthetic pigments, leading to an exponential attenuation of the screening at separations less than about 20 Å.[22,23]

While the PCM-LR methodology is well-suited to study EET in homogeneous solvents, the treatment of solvation in light-harvesting proteins is more challenging. Measurements of time-dependent fluorescence Stokes shifts[36] and molecular dynamics (MD) simulations[37] have shown that polar solvation dynamics in such systems are position-dependent and highly heterogeneous. Depending on the particular protein or protein site, for example, static dielectric permittivities ranging from 4 to 40 have been estimated from MD simulations.[38−41] In other words, the fine-tuning of the transition energies of the pigments that modulates the EET pathways as well as the screening effect on the couplings arise from different local pigment−protein interactions that cannot be captured by a continuum model. In addition, a continuum model directly provides ensemble-averaged quantities meaning that it is unable to describe the disorder in the transition energies and the electronic couplings due to the fluctuating environment, which are particularly important in the description of EET dynamics in multichromophoric arrays.[42,43]

In this paper we present a new combined quantum mechanical and molecular mechanical (QM/MM) method to study EET that overcomes the limitations of continuum models. In a QM/MM scheme, one part of the system (in this case the chromophores) is fully described at the QM level, whereas the solvent molecules or surrounding environment are described by a classical force field. QM/MM methods have successfully been applied to describe solvent effects on a variety of molecular properties including solvatochromic shifts in optical spectra.[44−49] The method we present here follows the same strategy used with PCM and it introduces a LR scheme to describe both chromophore excitations and EET couplings, while the environment is described through a MM force field. It is important to stress that an explicit treatment of electronic polarization in the environment is essential in order to account for screening effects on EET couplings: this effect is here recovered by using a polarizable MM force field. Below we will refer to this method as QM/MMpol.

We validate the method by comparing the results to "exact" calculations of the excitonic splitting in a model perylene diimide (PDI) dimer in water solution, in which the complete solute−solvent system is described at the QM level. In addition, QM/MMpol results averaged over solvent configurations sampled from MD simulations are compared to the predictions of the PCM-LR method, showing that both approaches are consistent and describe a similar distance-dependent decay of the solvent screening factor. Our results thus demonstrate the potential of the method to investigate the role of complex heterogeneous environments on EET.

The paper is organized as follows. In Section 2 we describe the theory underlying the method. In Section 3, we describe the computational details of the MD simulations and the QM/MMpol and PCM calculations. In addition, we report the derivation of the polarizable force field used to describe water in the QM/MMpol calculations. In Section 4, we first discuss the validity of the QM/MMpol model by comparing the results with exact QM supermolecule calculations of the complete solute−solvent system. Then, we compare solvent effects induced on transition properties as well as on the electronic couplings as described by the QM/MMpol and PCM-LR methods. Finally, in Section 5 we report our conclusions and give some perspectives on the potential of the method.

2. Methodology

2.1. Effective Hamiltonian for QM/MMpol. QM/MMpol and PCM belong to the same family of the so-called

"focussed models". The most important characteristic of both of them is in fact that the system is divided in two parts (or layers) which are described at different level of accuracy. The target layer (the solute plus eventually some solvent molecules) is described at the QM level (either ab initio or semiempirical), while the rest (the solvent) is approximated using a MM or a continuum description. In all cases, the formalism of *in vacuo* QM molecular calculations can be maintained if we introduce an effective Hamiltonian, H_{eff}, which includes an explicit term representing the solute−solvent interaction (and the energy of the MM region in the case of QM/MMpol). Introducing the standard Born−Oppenheimer approximation, the solute electronic wave function will satisfy the following equation

$$\hat{H}_{eff}|\Psi\rangle = (\hat{H}_0 + \hat{H}_{env})|\Psi\rangle = E|\Psi\rangle \quad (1)$$

where H_0 is the gas phase Hamiltonian of the QM solute system, and the operator H_{env} introduces the coupling between the solute and the solvent. What distinguishes MMpol from PCM is exactly the form of the operator H_{env}.

In the QM/MMpol approach we adopt here, the MM system is described by a classical polarizable force field based on the induced dipole model. In particular, electrostatic forces are described by atomic partial charges, whereas polarization is explicitly treated by adding isotropic polarizabilities at selected points in the solvent molecules. We thus have

$$\hat{H}_{env} = \hat{H}_{QM/MM} + \hat{H}_{MM} \quad (2)$$

and the solute−solvent interaction $\hat{H}_{QM/MM}$ and MM energy $\hat{H}_{MM}$ terms are given by

$$\hat{H}_{QM/MM} = \hat{H}^{el}_{QM/MM} + \hat{H}^{pol}_{QM/MM} = \sum_m q_m \hat{V}(r_m) - \frac{1}{2}\sum_a \mu_a^{ind} \hat{\mathbf{E}}_a^{solute}(r_a) \quad (3)$$

$$\hat{H}_{MM} = \hat{H}^{el}_{MM} + \hat{H}^{pol}_{MM} = \sum_m \sum_{n>m} \frac{q_m q_n}{r_{mn}} - \frac{1}{2}\sum_a \mu_a^{ind} \sum_m \frac{q_m(\mathbf{r}_a - \mathbf{r}_m)}{|\mathbf{r}_a - \mathbf{r}_m|^3} \quad (4)$$

where $\hat{V}(r_m)$ and $\hat{\mathbf{E}}_a^{solute}(r_a)$ are the electrostatic potential and electric field operators due to electrons and nuclei of the QM (solute) system at the MM sites, and the indexes *m (n)* and *a* run over the MM charges q_m and induced dipoles μ_a^{ind} located at r_m and r_a, respectively.

In eq 3, $H^{el}_{QM/MM}$ and $H^{pol}_{QM/MM}$ describe the interaction between the QM system and the MM charges and induced dipoles, respectively. On the other hand, in eq 4 H^{el}_{MM} describes the electrostatic self-energy of the MM charges, while H^{pol}_{MM} represents the polarization interaction between such charges and the induced dipoles. We recall that the H^{el}_{MM} term enters in the effective Hamiltonian only as a constant energetic quantity, while the H^{pol}_{MM} contribution is explicitly considered in the corresponding Fock operator because of the explicit dependence of the induced dipoles on the QM wave function. In addition, here we do not consider short-range dispersion and repulsion contributions in $H_{QM/MM}$ and H_{MM}, as in most combined QM/MM methods these are described by empirical potentials independent of the QM electronic degrees of freedom, thus not affecting our results.

The dipoles induced on each MM polarizable site are given by

$$\mu_a^{ind} = \alpha_a(\mathbf{E}_a^{solute} + \mathbf{E}_a^{solvent}\{\mathbf{q};\mu^{ind}\}) \quad (5)$$

where we have assumed a linear approximation, neglected any contribution of magnetic character related to the total electric field, and used an isotropic polarizability (α_a) for each selected point in the MM part of the system. In eq 5, $\mathbf{E}_a^{solvent}$ refers to the total solvent electric field calculated at site *a* and contains a sum of contributions from the point charges and the induced dipole moments in the MM part of the system. Such a field (and hence the induced dipole) depends on all other induced dipole moments in the solvent. This means that eq 5 must be solved iteratively within each SCF iteration. As an alternative, mutual polarization between the dipoles can be solved through a matrix inversion approach, where eq 5 is reformulated into a matrix equation

$$\boldsymbol{\mu}^{ind} = \mathbf{BE} \quad (6)$$

where the matrix **B** is of dimension 3N⊗3N, with N being the number of polarizable sites, and the vector **E** collects the electric field from the solute and the solvent permanent charge distribution. The form of matrix **B** will be determined uniquely by the position of the polarizable sites and the polarizability values.

Equation 6 is a further direct link between QM/MMpol and PCM; in PCM in fact the polarization of the solvent is expressed in terms of a set of apparent point charges placed on the surface of the molecular cavity embedding the QM system. These apparent charges are, exactly as the MMpol induced dipoles, determined by the electric field from the solute (or the electrostatic potential in more recent formulations of the model) calculated at the positions of the charges, namely

$$\mathbf{q}^{PCM} = -\mathbf{K}\mathbf{f}^{solute} \quad (7)$$

As the MMpol matrix **B**, also **K** is a square matrix (the dimension being now equal to Nts⊗Nts, where Nts is the number of apparent charges): it only depends on the geometrical cavity parameters and the dielectric constant of the solvent.

In both MMpol and PCM the addition of $\hat{H}_{env}$ to the solute Hamiltonian automatically leads to a modification of the solute wave function which has now to be determined by solving the effective eq 1. This can be done using exactly the same methods used for isolated molecules; here in particular we shall mainly focus on the standard Self Consistent Field (SCF) approach (either in its Hartree−Fock or DFT formulation). Due to the presence of $\hat{H}_{env}$ the modified SCF scheme is generally known as Self Consistent Reaction Field (SCRF), which emphasizes the mutually polarized solute−solvent system obtained at the end of the SCF. Historically the term SCRF has been coined for the

QM/Continuum approach, but here, due the parallelism between the two schemes, it will be used indistinctly for both.

2.2. QM/MMpol Linear Response. In the following we develop the working expressions to include the effects of the polarizable MM environment in a TD-DFT linear response scheme. Its extension to the Hartree−Fock or semiempirical level (TD-HF, CIS, or ZINDO) is straightforward. In this framework, the excitation energies of a molecular system can be determined by solving[50]

$$\begin{pmatrix} \mathbf{A} & \mathbf{B} \\ \mathbf{B}^* & \mathbf{A}^* \end{pmatrix}\begin{pmatrix} \mathbf{X}_n \\ \mathbf{Y}_n \end{pmatrix} = \omega_n \begin{pmatrix} 1 & 0 \\ 0 & -1 \end{pmatrix}\begin{pmatrix} \mathbf{X}_n \\ \mathbf{Y}_n \end{pmatrix} \tag{8}$$

where the matrices **A** and **B** form the Hessian of the electronic energy, and the transition vectors ($\mathbf{X}_n$ $\mathbf{Y}_n$) correspond to collective eigenmodes of the density matrix with eigenfrequencies ω_n. The Coulombic and exchange-correlation (XC) kernels produce both diagonal and off-diagonal contributions to **A** and **B**, correcting the transitions between occupied and unoccupied levels of the ground-state potential into the true transitions of the system. The effect of the polarizable environment on the **A** and **B** matrices can be included by considering the MM dipoles induced by the density matrix associated with the transition vectors ($\mathbf{X}_n$ $\mathbf{Y}_n$). The extension of this linear response scheme to include the effect of the MMpol environment is analogous to the inclusion of PCM solvent effects, which have been described in detail in ref 51. In the present case, the electronic part of the polarization response of the environment is represented by a set of point dipoles induced by the appropriate density matrix instead of a set of apparent surface charges displaced on the cavity surface as described in the PCM model.

By using the usual convention with respect to labeling the molecular orbitals (i.e., (i, j,...) for occupied; (a, b,...) for virtual), the matrices **A** and **B** thus become

$$A_{ai,bj} = \delta_{ab}\delta_{ij}(\varepsilon_a - \varepsilon_i) + K_{ai,bj} + C^{pol}_{ai,bj}$$

$$B_{ai,bj} = K_{ai,jb} + C^{pol}_{ai,bj} \tag{9}$$

where ε_r are the orbital energies, and $K_{ai,bj}$ and $C^{pol}_{ai,bj}$ are the coupling matrix and the polarizable MM matrix, respectively

$$K_{ai,bj} = \int d\mathbf{r}\int d\mathbf{r}'\phi_i(\mathbf{r}')\phi_a^*(\mathbf{r}')\left(\frac{1}{|\mathbf{r}'-\mathbf{r}|} + g_{xc}(\mathbf{r}',\mathbf{r})\right)\phi_j(\mathbf{r})\phi_b^*(\mathbf{r}) \tag{10}$$

$$C^{pol}_{ai,bj} = -\sum_k\left(\int d\mathbf{r}\phi_i(\mathbf{r})\phi_a^*(\mathbf{r})\frac{(\mathbf{r}_k - \mathbf{r})}{|\mathbf{r}_k - \mathbf{r}|^3}\right)\mu_k^{ind}(\phi_j\phi_b^*) \tag{11}$$

and g_{xc} is the exchange eventually plus correlation (if a DFT description is used) kernel. In eq 11 the k index runs on the total number of polarizable MM sites. We note that for CIS and ZINDO the whole matrix **B** is neglected, and for ZINDO the xc terms in eq 10 become zero.

2.3. Electronic Energy Transfer Coupling. We begin by considering two solvated chromophores, A and D, with a common resonance frequency, ω_0, when not interacting. When the interaction is turned on, their respective transitions are no longer degenerate. Instead, two distinct transition frequencies ω_+ and ω_- appear, and the excited states become delocalized over the two monomers. The splitting between these defines the energy transfer coupling, V

$$V = \frac{(\omega_+ - \omega_-)}{2} \tag{12}$$

Such a splitting can be evaluated by computing the excitation energies of the $D\oplus A$ system through a TD-DFT scheme, as shown in the previous section. This procedure to estimate electronic couplings is known as the "supermolecule" approach.

An approximate solution to eq 12, however, can be obtained by introducing a perturbative approach which considers the D/A interaction as a perturbation and defines the zero-order resulting eigenvectors, ($\mathbf{X}_+$ $\mathbf{Y}_+$) and ($\mathbf{X}_-$ $\mathbf{Y}_-$), as linear combinations of the unperturbed Kohn−Sham orbitals of the isolated D and A systems.[52] In analogy to the PCM-LR method for EET,[31] this approximation allows the estimation of the splitting and the corresponding coupling from the transition densities calculated for the noninteracting D and A. To first order, the electronic coupling, V, is obtained as a sum of two terms

$$V = V_s + V_{\text{explicit}} \tag{13}$$

$$V_s = \int d\mathbf{r}\int d\mathbf{r}'\rho_A^{T^*}(\mathbf{r}')\left(\frac{1}{|\mathbf{r}'-\mathbf{r}|} + g_{xc}(\mathbf{r}',\mathbf{r})\right)\rho_D^T(\mathbf{r}) - \omega_0\int d\mathbf{r}\rho_A^{T^*}(\mathbf{r})\rho_D^T(\mathbf{r}) \tag{14}$$

$$V_{\text{explicit}} = -\sum_k\left(\int d\mathbf{r}\rho_A^{T^*}(\mathbf{r})\frac{(\mathbf{r}_k - \mathbf{r})}{|\mathbf{r}_k - \mathbf{r}|^3}\right)\mu_k^{ind}(\rho_D^T) \tag{15}$$

where ρ_D^T and ρ_A^T indicate transition densities of the solvated D and A, respectively, in the absence of their interaction.

In eq 13, V_s describes a chromophore−chromophore Coulomb and exchange-correlation interaction corrected by an overlap contribution. This term is the only one present in vacuum but can be significantly modified upon solvation due to changes induced by the environment in the transition densities, such effect in general leading to an enhancement of the coupling.[23] On the other hand, $V_{explicit}$ describes the interaction between D and A mediated by the polarizable environment. This contribution typically reduces, i.e. *screens*, the overall interaction and is given by the interaction between ρ_A^T and the MM dipoles induced by ρ_D^T (the same result is obtained by exchanging A with D as the term is symmetric with respect to the transition densities). As introduced in our previous studies,[22,23] we can now define the solvent screening factor as

$$s = \frac{V}{V_s} = \frac{V_s + V_{\text{explicit}}}{V_s} \tag{16}$$

which can be directly compared to the $s = 1/n^2$ factor used in Förster's model.

Finally, we note that in the case of an asymmetric system, where the transition energies ω_D and ω_A of the noninteracting monomers are not equal, such asymmetry has to be taken

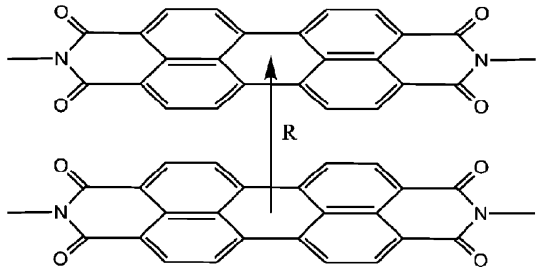

Figure 1. Structure of the perylene diimide (PDI) dimer considered in this work. Two interchromophoric distances (R=3.5 and R=7.0 Å) corresponding to a face-to-face orientation were considered.

into account when deriving the coupling from the energy splitting. This case is relevant for the "supermolecule" calculations we present in Section 4.1. The corresponding expression can be derived from the secular determinant describing Frenkel excitons by considering two-level chromophores[53]

$$V = \frac{1}{2}\sqrt{(\omega_+ - \omega_-)^2 - (\omega_D - \omega_A)^2} \qquad (17)$$

It is obvious that for identical ω_D=ω_A we recover the initial expression, eq 12. The contribution of other electronic states to the splitting may not be neglected, but this problem is minimized in the case of nearly identical PDI molecules as considered in this work, where the asymmetry arises only from slightly different local interactions with the solvent.

3. Computational Details

3.1. Molecular Dynamics Simulations. The systems made of two PDI stacked molecules placed in parallel orientation (see Figure 1) at a distance of 3.5 and 7.0 Å (hereafter named mod35 and mod70, respectively) were inserted in rectangular parallelepiped boxes and solvated with polarizable POL3 water molecules[54] removing those waters falling within 1.5 Å from the adducts. All simulations were performed using the AMBER9 package with the general amber force field (GAFF)[55] to describe the solute. Before production simulations were started, the cell size for both adducts was adjusted in a series of minimizations and short NVT molecular dynamics simulation runs in order to achieve the correct density of the water molecules filling the simulation box. The final box dimensions and the corresponding water molecules were $37.4 \times 28.4 \times 27.4$ Å^3 (937 waters) and $37.0 \times 28.4 \times 30.2$ Å^3 (1055 waters) for mod35 and mod70, respectively.

Then pre-equilibration in the NVT ensemble was performed first at high temperature ($T = 600$ K), in order to randomize water positions, and then at lower temperature ($T = 298$ K). The Andersen temperature coupling scheme[56] with a relaxation time of 0.4 ps was employed. The solute was kept fixed at the initial geometry during all the simulations. The time step was set to 1 fs. Periodic boundary conditions were applied, and the particle mesh Ewald method[57] was used to deal with electrostatic forces. Starting from the last obtained equilibrium configuration, production runs were performed in the NVT ensemble for a total simulation time of 2 ns. Configurations were saved every picosecond for subsequent QM and QM/MMpol calculations. In particular, QM/MM results presented on Section 4.2 correspond to 100 structures saved every 20 ps, which we found to be enough to obtain converged results.

3.2. Definition and Determination of Partial Atomic Charges and Distributed Polarizabilities Used in QM/MMpol Calculations. As described in the previous section, MD simulations were performed adopting the polarizable POL3 water model.[54] While this model has been optimized to reproduce bulk structural properties of water, it substantially underestimates the water polarizability (see ref 58 for a detailed discussion). It is therefore not adequate to study electronic properties, so we derived new sets of partial atomic charges and distributed polarizabilities to be used in the QM/MMpol calculations. In particular, the distributed atomic dipole−dipole polarizabilities were calculated using the LoProp[59] approach as implemented in the Molcas[60] program, whereas the atomic charges were fitted to the electrostatic potential following the ESP method implemented in the GAUSSIAN package.[61] The calculations were performed at either the level of Hartree−Fock or DFT employing the B3LYP density functional. The basis set used were either the 6-31G(d) or the aug-cc-pVTZ. However, for the LoProp to be properly defined, these basis sets were first transformed into the atomic natural orbital form by a linear transformation which does not affect the orbital optimization. The expansion points used for water were either (i) at the atomic nuclei or (ii) at the atomic nuclei and the bond midpoints. However, test calculations indicated that the effect of the local properties was equally described using either approaches, and since the number of polarizable sites is reduced by expanding only at the atomic nuclei, this approach was taken by us in the final and reported calculations. In all property calculations a single water monomer at the POL3 geometry was considered. This means that intramolecular polarization is included automatically in the derived force field parameters and the multipole-induced dipole, and, in the QM/MMpol calculations, induced dipole−induced dipole interactions are thereby only explicitly considered between different water molecules. In this way only intermolecular distances are relevant, and damping functions related to the electric field were therefore not considered. In addition, the induced dipoles were in the QM/MMpol calculations solved by a matrix inversion procedure, as indicated by eq 6, and no artificially large water induced dipoles were observed. The sets of atomic charges and isotropic polarizabilities (in atomic units) obtained were as follows: i) HF/6-31G(d): $\alpha_O = 2.94$, $\alpha_H = 1.18$, $q_O = -0.78$, $q_H = 0.39$; ii) B3LYP/aug-cc-pVTZ: $\alpha_O = 5.74$, $\alpha_H = 2.31$, $q_O = -0.64$, $q_H = 0.32$. We note that the HF/6-31G(d) set of parameters is very similar to the POL3 water model, and test calculations showed very similar results using one or the other. However, we preferred to adopt the HF set in order to perform a fair comparison to full QM CIS/6-31G(d) calculations, as described below. All QM/MMpol calculations were performed in a locally modified version of Gaussian.

3.3. PCM Calculations. The only parameters needed in the PCM model are the positions and radii of the spheres

determining the cavity embedding the molecule and the environment optical (ε_{opt}) and static (ε_0) permittivities. PCM cavities have been constructed by applying the united atom topological model and the atomic radii of the UFF[62] force field as implemented in the GAUSSIAN 03 code.[61] Transition energies, transition densities, and electronic couplings have been obtained by considering a single cavity enclosing the *D*/*A* pair for the 3.5 Å interchromophoric distance and two distinct cavities (one for each chromophore) for the 7.0 Å distance. As here the PCM has to mimic water, we have used the permittivities experimentally known for water, namely $\varepsilon_{opt} = 1.776$ and $\varepsilon_0 = 78.39$.

4. Results

4.1. Comparison between QM/MMpol and Full QM Supermolecule Calculations. In this section, we validate the QM/MMpol model by comparison with exact supermolecule calculations of the complete solute−solvent system described at a full quantum-mechanical level. Such full QM calculations are computationally very expensive, so we limit the analysis to a single solute−solvent configuration extracted from the MD simulations. This is in contrast to the ensemble averaged quantitities that we will present in the next section. Moreover, even for a single snapshot one must include a very large number of solvent molecules in order to get converged results due to the long-range nature of electrostatic interactions. For the PDI dimer in water, test calculations indicate that convergence below 1% error on electronic couplings and solvent screening factors is achieved by including the water molecules located inside a hypothetical sphere of cutoff radius of ∼19 Å from the center of the dimer; this corresponds to ∼800 water molecules. We also note that the convergence is faster for transition energies and dipoles. Due to the high computational cost of the full QM calculations, for this first part of the analysis we have to use smaller cutoff values (in the range 7−11 Å).

For the same reason, MMpol and full QM calculations are performed with a single level of theory (CIS/6-31G(d)), whereas in the next section ZINDO and time-dependent density functional theory (TD-DFT) results will also be presented. The main reason for choosing CIS instead of TDDFT is related to the problem of the large number of artificial low-lying charge-transfer states that the surrounding waters introduced in full QM TD-DFT calculations. Such a problem arises from the well-known deficiencies of most of the present exchange-correlation functionals[63] and strongly complicates the determination of the dimer states of interest. In contrast, at the CIS level, the states of interest are the first two excited states.

As already noted in the Introduction, a proper description of electronic polarization is crucial in order to describe the effect of the environment on the electronic coupling. It is well-known that extended basis sets are needed in QM methods in order to properly describe polarization. Again, the cost of the full QM calculations limits us to use a split-valence 6-31G(d) basis set, which is expected to recover only part of the polarization effect on the coupling. In order to be consistent in the treatment of polarization in the full QM and the QM/MMpol calculations, we have thus developed a MM polarizable force-field of water derived from HF/6-31G(d) calculations, as described in Section 3.2. This allows us to perform a fair and consistent comparison between the MM and QM descriptions of the environment. We are however aware of the deficient treatment of polarization effects at this level of theory; this is clearly illustrated by the fact that the experimental polarizability of water is approximately two times the value predicted at the HF/6-31G(d) level. Thus, we have also developed an accurate force field of water from B3LYP/aug-cc-pVTZ calculations, which in turn provides a set of atomic polarizabilities that accurately describe the experimental polarizability of water.

Table 1. CIS/6-31G(d) Electronic Coupling and Solvent Screening Factors Calculated with the Perturbative QM/MMpol Model and from Exact Supermolecule Calculations of the Full QM Solute-Solvent System[b]

	MMpol (HF/6-31G(d) derived force field)				
cutoff (Å)[a]	V_s	$V_{explicit}$	V	s	full QM V
7	585	−5	580	0.99	569
8	590	−25	565	0.96	550
9	604	−45	560	0.93	547
10	605	−56	549	0.91	540
11	610	−70	541	0.89	534

	MMpol (B3LYP/aug-cc-pVTZ derived force field)				
cutoff (Å)[a]	V_s	$V_{explicit}$	V	s	full QM V
7	599	−27	572	0.95	569
8	610	−68	542	0.89	550
9	629	−105	524	0.83	547
10	633	−126	507	0.80	540
11	639	−148	492	0.77	534

[a] Increasing cutoff distances correspond to the consideration of 21, 46, 80, 108, and 159 number of water molecules in the system. [b] Results corresponding to an interchromophoric distance of 7.0 Å are given as a function of the cutoff distance determining the number of waters included in the calculation. Two different sets of MMpol parameters (charges and atomic polarizabilities), derived at the HF/6-31G(d) and B3LYP/aug-cc-pVTZ level, are used to describe the MM environment. All couplings are in cm^{-1}.

In Table 1 we show the results obtained from the full QM CIS/6-31G(d) calculations as well as the perturbative couplings obtained from CIS/6-31G(d)/MMpol calculations by adopting the two different polarizable force fields. The calculations have been performed for a dimer at an interchromophoric distance of 7.0 Å, because, at this distance, solvent screening effects are expected to be more significant than at smaller separations. Full QM couplings are derived from the splitting of the dimer excited states corrected by the mismatch in the donor−acceptor energies, as indicated by eq 17. This implies a QM calculation on the complete dimer-solvent system to obtain ω_+ and ω_- as well as two calculations on the donor-solvent (acceptor-solvent) system, where the other chromophore has been removed, in order to estimate ω_D (ω_A).

The computed couplings in Table 1 clearly show than when a consistent treatment of polarization is used in the QM and MM descriptions through the HF-derived force field, the MMpol model accurately reproduces solvent effects on the coupling, with error in the electronic coupling being always <3%, which corresponds to <15 cm^{-1}. Such behavior

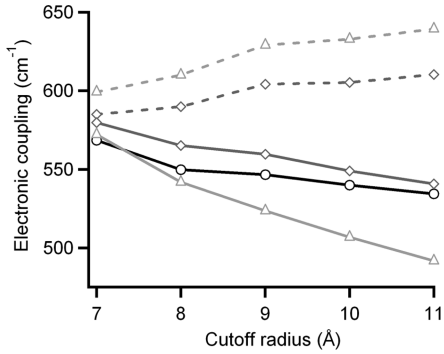

Figure 2. CIS/6-31G(d) electronic couplings obtained from full QM calculations (circles) and from QM/MMpol calculations using the HF/6-31G(d) (diamonds) and the B3LYP/aug-cc-pVTZ (triangles) force fields, represented as a function of the cutoff radius determining the number of water molecules in the system. Solid lines correspond to the total electronic coupling, V, and dashed lines correspond to the unscreened Coulombic contribution, V_s.

is achieved because the QM/MMpol model seems to capture both implicit and explicit screening effects on the coupling in a balanced way, as illustrated in Figure 2. That is, when the number of solvent molecules in the system is increased, the change in the transition densities upon solvation is reflected in a significant enhancement of the direct Coulombic interaction between D/A, V_s, which passes from 585 to 610 cm^{-1}. At the same time, however, the solvent-mediated term goes from -5 to -70 cm^{-1}, thus resulting in an overall reduction or screening of the total interaction. Thus, the MMpol model also provides physical insights on the solvent-induced changes on the coupling, which are not possible from the supermolecule calculations.

It is also worth mentioning that throughout the cutoff range considered, where the number of solvent molecules is increased from 21 to 159, the error in the estimated coupling stays relatively constant, close to $\sim$10 cm^{-1}, suggesting that the small differences observed between the two approaches could arise from short-range dispersion/repulsion effects neglected in the MMpol model. In addition, we want to note that at the distance considered here (R = 7 Å), the differences observed between MMpol and full QM results arise because of the different treatment of the environment and not because of the perturbative approach used to estimate the coupling. This has been checked by computing the exact supermolecule coupling also from QM/MMpol calculations, and the differences between the exact (eq 17) and the approximate values (eq 13) were always less than 1%.

On the other hand, the results obtained with the DFT-derived force field illustrate the importance of accurately describing solvent polarization in the estimation of the coupling. As noted above, this set of atomic polarizabilities describe a water molecular polarizability ($\alpha = 1.53$ Å^3) close to the experimental value ($\alpha_{exp} = 1.44$ Å^3), whereas the HF-derived set accounts for only one-half of it ($\alpha = 0.78$ Å^3). As a result, both the enhancement of the Coulombic coupling and the screening contribution induced by the solvent are strongly enlarged with these new polarizabilities, as reflected in Table 1. For the largest cutoff considered, the change involves 49 cm^{-1}, corresponding to a 10% change in the total coupling. Moreover, this change represents a 111% enlargement of the solvent-mediated contribution, which significantly modifies the solvent screening factor from $s = 0.89$ to 0.77. We note that the effect of the charges used to describe water is far less significant than the set of atomic polarizabilities. For instance, test calculations adopting the DFT set of polarizabilities but the charges of the POL3 force field induced only minor $\sim$1% changes in the total coupling.

It is also interesting to investigate the differential solvatochromic shifts on the donor and acceptor transition energies obtained from a QM and MMpol descriptions of the environment, as this has important consequences on the localization/delocalization character of the dimer excited states. As we consider a single solvent configuration in this section, the slightly different solvent structure surrounding D and A induces a mismatch in their transition energies. In Table 2 we show the transition energies obtained from the QM/MMpol and full QM calculations for the donor (ω_D) and acceptor (ω_A) as well as the corresponding energy difference between them (ω_D - ω_A). The results indicate that the MMpol model correctly describes the lowest-energy chromophore in all cases. In addition, the difference ω_D -ω_A is reproduced reasonably well, in particular when the HF-derived parameters consistent with the QM level of theory are used. This is illustrated by the fact that the observed errors in this latter case, about $\sim$0.01 eV, are reasonably small compared to the absolute magnitude of the solvatochromic shifts, which are 0.05 (0.08) eV and 0.07 (0.10) eV for the donor (acceptor) as given by the QM/MMpol and full QM calculations, respectively. These shifts are estimated from the reference vacuum transition energy, equal to 3.31 eV. The ability of the MMpol model to describe the relative fine-tuning of the transition energies induced by different local environments is in fact an important feature of the model, because in multichromophoric protein systems such local interactions can strongly modulate the EET pathways.[64]

4.2. Comparison between QM/MMpol and PCM. Once the QM/MMpol approach is validated with exact QM supermolecule results, we proceed to compare solvent effects on both transition properties and electronic couplings as described by the MMpol and PCM methods. In order to explore the distance-dependence behavior of solvent screening effects, two interchromophore distances, 3.5 Å and 7 Å, are considered. For this analysis we have used the B3LYP/aug-cc-pVTZ set of charges and polarizabilities, which accurately describe the aqueous polarizable environment as discussed in the previous section. In addition, results are averaged over 100 different solvent configurations extracted from the MD trajectories, which we found to be enough to obtain converged results. The standard deviation in transition energies, dipoles, and total electronic couplings was less than 2% in all cases.

Transition energies and transition dipole moments calculated in vacuo and in aqueous solution are reported in Table 3 for both QM/MMpol and PCM models at ZINDO, CIS, and TD-B3LYP levels. We note that due to the ensemble-averaging, equivalent properties are obtained for D and A, so a single set of values is reported.

Table 2. CIS/6-31G(d) Donor and Acceptor Transition Energies Calculated from the QM/MMpol Model and from Full QM Calculations of the Chromophore-Solvent System[b]

	MMpol (HF force field)			MMpol (B3LYP force field)			full QM		
cutoff (Å)[a]	ω_D	ω_A	ω_D - ω_A	ω_D	ω_A	ω_D - ω_A	ω_D	ω_A	ω_D -ω_A
7	3.28	3.27	0.01	3.26	3.26	0.01	3.27	3.25	0.01
8	3.28	3.26	0.02	3.24	3.24	0.01	3.26	3.23	0.03
9	3.27	3.24	0.04	3.23	3.20	0.03	3.26	3.21	0.05
10	3.27	3.23	0.03	3.22	3.19	0.03	3.25	3.21	0.05
11	3.26	3.23	0.03	3.21	3.19	0.02	3.24	3.21	0.04

[a] Increasing cutoff distances correspond to the consideration of 21, 46, 80, 108, and 159 number of water molecules in the system. [b] Results given as a function of the cutoff distance determining the number of waters included in the calculation. Two different sets of MMpol parameters (charges and atomic polarizabilities), derived at the HF/6-31G(d) and B3LYP/aug-cc-pVTZ level, are used to describe the MM environment. All energies are in eV.

Table 3. Transition Energies (in eV) and Transition Dipole Moments (in Debye) for PDI in Vacuum and in Aqueous Solution Calculated at the ZINDO, CIS/6-31G(d), and TD-B3LYP/6-31G(d) Levels from the QM/MMpol and PCM Methods

	ZINDO		CIS		TD-B3LYP	
	ΔE	μ^T	ΔE	μ^T	ΔE	μ^T
vacuum	2.60	10.9	3.31	9.9	2.43	8.5
MMpol	2.39	12.0	3.18	10.7	2.31	9.7
PCM	2.37	12.1	3.19	10.6	2.32	9.7

As expected from the $\pi-\pi^*$ nature of the excitation, a red shift is found passing from vacuum to aqueous solution (0.21, 0.13, and 0.12 eV for ZINDO, CIS and TD-B3LYP, respectively). Similar red shifts were obtained in a previous study of PDI in toluene.[33] The $\pi\rightarrow\pi^*$ character of the transition also explains the transition dipole moment orientation along the main longitudinal axis of the planar structure of the PDI, shown in Figure 1. The solvent does not affect the orientation of the transition dipole moment but increases its magnitude by about 10, 8, and 14% for ZINDO, CIS, and TD-B3LYP, respectively.

In Table 4 we show the ZINDO, CIS, and TD-B3LYP electronic couplings obtained in vacuo and in water with either the MMpol or the PCM models. The tables report the total value of the coupling and its two contributions, V_s and $V_{explicit}$ (see eqs 14 and 15). We recall that V_s contains different terms, Coulombic, exchange (eventually plus correlation in the case of TD-DFT), and overlap. In all cases overlap is negligible, whereas exchange(-correlation) terms represent ~5% of the total coupling in the CIS results at R = 3.5 Å, and ~1% in all other cases.

As we have shown in a previous study,[33] TD-B3LYP tends to underestimate the electronic coupling by about 20−25% when compared to more accurate SAC-CI results, while ZINDO presents a more unpredictable behavior depending on the particular system under study. We found that ZINDO coupling values for PDI are in good agreement with SAC-CI values. In the same study we have also found that the coupling values do not significantly depend on the chosen basis set. On the basis of such findings, we have limited here our analysis to the 6-31G(d) basis set; this in fact represents a good compromise between accuracy and computationally efficiency (we recall that each MMpol result implies an average on 100 calculations).

As expected, when the solvent is introduced we observe a net decrease of the coupling (about 25, 20, and 15% for ZINDO, CIS, and TD-B3LYP, respectively); this is due to the screening effect here quantified in terms of the factor s that relates the total coupling with the unscreened Coulombic contribution (eq 16). In addition, the solvent screening factor s decreases in all cases when the *D*/*A* separation is increased. At R = 3.5 Å, in fact, the solvent cannot penetrate between the two chromophores, and as a result the screening is reduced. Thus, the factor s is lower for the larger distance (0.72 and 0.67 for 3.5 and 7.0 Å, respectively for TD-B3LYP results).

Let us now compare MMpol with PCM. Concerning transition energies and dipole moments reported in Table 3, MMpol and PCM show very similar behaviors. This seems to indicate that in the present system, possible effects due to specific short-range solute−solvent interactions (such as hydrogen-bonding) do not significantly affect the transition properties and that an averaged picture as the one represented by the PCM is not only accurate enough but also realistic in terms of the description of the main solvent effects.

Moving to the coupling values, once again MMpol compare well with PCM values at all QM levels, with PCM results being always slightly smaller than MMpol. This behavior is due to larger screening contributions obtained by PCM with respect to MMpol (the Coulombic terms are in fact very similar in the two models). This is reflected in the factor s which is always smaller in the PCM description, that is, the screening effect of the solvent in PCM is always larger than in MMpol.

In order to better appreciate these similarities between MMpol and PCM, we have, however, to analyze some numerical aspects. In the PCM model we have to define the cavity embedding the molecular system; this is generally done by defining the cavity as an envelope of spheres centered on selected atoms. As in all continuum models, PCM results will depend on the parameters used to define such a cavity (in particular, the radii used for the spheres). To check how this dependency can affect the results presented in Table 4 we have repeated the PCM calculations using different cavities obtained by scaling the default radii by different factors, namely $f = 1.1$, 1.2, and 1.3. The results obtained for the coupling are reported in Table 5 (for this analysis only ZINDO and TDDFT are presented)

By comparing the results of Tables 4 and 5, two different effects of such a tuning of the cavity are observed at the

Table 4. ZINDO, CIS/6-31G(d), and TD-B3LYP/6-31G(d) Electronic Couplings and the Corresponding Screening Factors *s* Calculated for the PDI Dimer in Aqueous Solution from the QM/MMpol and PCM Methods[a]

	ZINDO				CIS/6-31G(d)				TD-B3LYP/6-31G(d)			
	V_s	$V_{explicit}$	V	s	V_s	$V_{explicit}$	V	s	V_s	$V_{explicit}$	V	s
						Distance 3.5 Å						
vacuum	1359		1359		1642		1642		1086		1086	
MMpol	1579	−543	1036 (−24)	0.65	1805	−457	1348 (−18)	0.75	1282	−356	926 (−15)	0.72
PCM	1603	−608	994 (−27)	0.62	1813	−504	1309 (−20)	0.72	1294	−390	904 (−17)	0.69
						Distance 7.0 Å						
vacuum	567		567		571		571		399		399	
MMpol	693	−257	436 (−23)	0.63	661	−215	446 (−22)	0.68	508	−168	340 (−15)	0.67
PCM	711	−280	431 (−24)	0.61	660	−228	432 (−24)	0.65	514	−182	332 (−17)	0.65

[a] The values in parentheses refer to percent variations with respect to vacuum. All couplings are in cm^{-1}.

Table 5. PCM EET Couplings Calculated for the PDI Dimer in Aqueous Solution at the ZINDO and TD-B3LYP/6-31G(d) Levels[a]

	ZINDO				TD-B3LYP/6-31G(d)			
f	V_s	$V_{explicit}$	V	s	V_s	$V_{explicit}$	V	s
			Distance 3.5 Å					
1.1	1563	−544	1020 (−25)	0.65	1264	−351	913 (−16)	0.72
1.2	1534	−489	1045 (−23)	0.68	1241	−317	924 (−15)	0.74
1.3	1510	−442	1068 (−21)	0.71	1223	−288	935 (−14)	0.76
			Distance 7.0 Å					
1.1	688	−265	424 (−25)	0.62	499	−172	327 (−18)	0.65
1.2	670	−250	420 (−26)	0.63	487	−158	324 (−19)	0.67
1.3	656	−243	413 (−27)	0.63	476	−150	319 (−20)	0.67

[a] The three sets of data correspond to three different cavities (see text for details). All couplings are in cm^{-1}.

two interchromophore distances. For the distance of 3.5 Å, the total coupling increases with the factor *f*, while for the distance of 7.0 Å, the total coupling decreases when the factor *f* is larger. To understand this difference we have to recall that, for the 3.5 distance, the PCM calculations are done with a single cavity that embeds the two monomers; there is no solvent between the molecules. So, when the factor *f* increases, both coupling terms decrease but the screening one to a greater extent. In other words, by enlarging the cavity there is a smaller enhancement of the Coulombic interaction upon solvation, but the decrease of screening effects is even greater so that the balance between both contributions leads to a small overall increase in the coupling. It seems that the best agreement in the total coupling between PCM and MMpol is obtained for *f* equal to 1.2; however, if we analyze the single components and the screening factor *s*, the best agreement is found for $f = 1.1$. On the other hand, for the distance of 7.0 Å, we have two separated cavities for the two monomers so we can expect that the dominant changes at large *f* are in the Coulombic contribution and not in the screening one as found for the short distance. In addition, at this distance the solvent screening factor is significantly less sensitive to the particular definition of the PCM cavity through the factor *f*.

Finally, we discuss in some detail the computational cost associated with the introduction of solvent effects through the PCM and MMpol methods. At the CIS/6-31G(d) level, the total CPU time associated with the calculation of the coupling relative to the vacuum calculation was 1.4/3.2 (R = 3.5 Å) and 1.5/8.6 (R = 7.0 Å) for MMpol/PCM, respectively. This illustrates the fact that the cost associated with the QM/MMpol method is quite insensitive to the D−A separation, as the number of induced dipoles considered is kept relatively constant. In contrast, the cost associated with the PCM calculation increases substantially when passing to R = 7.0 Å, because in this case two different cavities host the chromophores, thus increasing the number of apparent surface charges displaced on the cavity surface. This is because in both methods, the added computational cost is mainly originated by the matrix inversion step needed to obtain the **B** and **K** matrices in eqs 6 and 7, respectively. Note also that if higher QM levels of theory are used, the relative cost added to the vacuum calculation is expected to be smaller. We also remark that the above timings refer to a single QM/MMpol calculation, whereas in general one has to perform a proper ensemble-average over several solute−solvent configurations. In this work, we considered 100 solute−solvent structures, and coupling values (transition energies) fluctuated over a ∼40 cm^{-1} (∼50 meV) range in the above-mentioned CIS calculations. Nevertheless, convergence in this system was very fast, and averaging over 25 structures already gave results converged below 1 cm^{-1} (2 meV).

To summarize, we find that the QM/MMpol method describes solvent effects both on transition properties and on the coupling in a very similar way to PCM despite the completely different description of the solvent characterizing the two models. Moreover, it is very remarkable that the *change* in the solvent screening factor when the interchromophoric distance is enlarged from 3.5 Å to 7.0 Å is almost the same as predicted by a continuum dielectric and an explicit discrete representation of the environment, a finding which strongly supports the distance-dependent screening function we have recently proposed based on PCM calculations.[22,23]

5. Conclusions and Perspectives

We have presented a novel polarizable QM/MM method to study EET in condensed phase. The method is based on a linear response approach, and it has been implemented at the semiempirical (ZINDO), Hartree−Fock (CIS), and density functional theory (TD-DFT) levels. This approach allows an atomistic description of environment effects on all quantities determining EET, i.e. chromophores' transition energies and dipoles, and on the electronic couplings. The method has been tested on a model PDI dimer in water

solution; we have found an excellent agreement between the QM/MMpol method and "exact" supermolecule calculations in which the complete solute−solvent system is described at the QM level. Our results also indicate that the estimation of the electronic coupling is extremely sensitive to the treatment of the solvent polarization and that an accurate set of parameters for the polarizable force field is necessary. On the other hand, the accuracy of the results predicted using the PCM model are found to be very sensitive to the exact shape and size of the molecular cavity imposing in this respect the problem of defining the most physically correct cavity. Finally, we have compared QM/MMpol results averaged over solvent configurations sampled from MD simulations to the corresponding ones obtained using the PCM-LR method, which is based on a continuum dielectric description of the solvent. We have shown that both continuum and atomistic solvent models describe similar solvent effects on EET in homogeneous media such as water. Most notably, both approaches describe a consistent decay of solvent screening as a function of donor−acceptor separation. This latter finding strongly supports the empirical distance-dependent screening function we recently derived from PCM-LR calculations.[22,23]

All these results demonstrate the reliability and robustness of the polarizable QM/MM method, and they make us confident in its potential to investigate the role of complex heterogeneous environments on EET, e.g. proteins or nanostructured host materials, where a continuum description of the environment represents an important limitation.

Acknowledgment. The work in Toronto was supported by the Natural Sciences and Engineering Research Council of Canada. G.D.S. acknowledges the support of an E. W. R. Steacie Memorial Fellowship. A.M.L. thanks support from the Spanish Ministerio de Ciencia e Innovación (Programa Nacional de Recursos Humanos del Plan Nacional I-D+I 2008-2011). J.K. thanks the Danish Natural Science Research Council/The Danish Councils for Independent Research and the Villum Kann Rasmussen foundation for financial support. B.M. wishes to thank Gaussian Inc. for financial support.

References

(1) Scholes, G. D. *Annu. Rev. Phys. Chem.* **2003**, *54*, 57.

(2) Fleming, G. R.; Scholes, G. D. *Nature* **2004**, *431*, 256.

(3) Sundstrom, V.; Pullerits, T.; van Grondelle, R. *J. Phys. Chem. B* **1999**, *103*, 2327.

(4) van Amerongen, H.; Valkunas, L.; van Grondelle, R. *Photosynthetic Excitons*; World Scientific Publishers: Singapore, 2000.

(5) Gust, D.; Moore, T. A.; Moore, A. L. *Acc. Chem. Res.* **2001**, *34*, 40.

(6) Jolliffe, K. A.; Bell, T. D. M.; Ghiggino, K. P.; Langford, S. J.; Paddon-Row, M. N. *Angew. Chem., Int. Ed.* **1998**, *37*, 915.

(7) Balzani, V.; Campagna, S.; Denti, G.; Juris, A.; Serroni, S.; Venturi, M. *Acc. Chem. Res.* **1998**, *31*, 26.

(8) Holten, D.; Bocian, D. F.; Lindsey, J. S. *Acc. Chem. Res.* **2002**, *35*, 57.

(9) Lee, J.-I.; Kang, I.-N.; Hwang, D.-H.; Shim, H.-K.; Jeoung, S. C.; Kim, D. *Chem. Mater.* **1996**, *8*, 1925.

(10) List, E. J. W.; Holzer, L.; Tasch, S.; Leising, G.; Scherf, U.; Müllen, K.; Catellani, M.; Luzzati, S. *Solid State Commun.* **1999**, *109*, 455.

(11) Wang, H.-L.; McBranch, D. W.; Klimov, V. I.; Helgeson, R.; Wudl, F. *Chem. Phys. Lett.* **1999**, *315*, 173.

(12) Brédas, J. L.; Beljonne, D.; Coropceanu, V.; Cornil, J. *Chem. Rev.* **2004**, *104*, 4971.

(13) Jares-Erijman, E.; Jovin, T. M. *Nat. Biotechnol.* **2003**, *21*, 1387.

(14) Lippincott-Schwartz, J.; Snapp, E.; Kenworthy, A. *Nat. Rev. Mol. Cell. Biol.* **2001**, *2*, 444.

(15) Weiss, S. *Nat. Struct. Biol.* **2000**, *7*, 724.

(16) Förster, T. *Ann. Phys.* **1948**, *2*, 55.

(17) Beljonne, D.; Curutchet, C.; Scholes, G. D.; Silbey, R. J. *J. Phys. Chem. B* **2009**, *113*, 6583.

(18) Krueger, B. P.; Scholes, G. D.; Fleming, G. R. *J. Phys. Chem. B* **1998**, *102*, 5378.

(19) Beljonne, D.; Cornil, J.; Silbey, R.; Millie, P.; Bredas, J. L. *J. Chem. Phys.* **2000**, *112*, 4749.

(20) Wong, K. F.; Bagchi, B.; Rossky, P. J. *J. Phys. Chem. A* **2004**, *108*, 5752.

(21) Beenken, W. J. D.; Pullerits, T. *J. Chem. Phys.* **2004**, *120*, 2490.

(22) Scholes, G. D.; Curutchet, C.; Mennucci, B.; Cammi, R.; Tomasi, J. *J. Phys. Chem. B* **2007**, *111*, 6978.

(23) Curutchet, C.; Scholes, G. D.; Mennucci, B.; Cammi, R. *J. Phys. Chem. B* **2007**, *111*, 13253.

(24) Pullerits, T.; Freiberg, A. *Chem. Phys.* **1991**, *149*, 409.

(25) Pullerits, T.; Hess, S.; Herek, J. L.; Sundstrom, V. *J. Phys. Chem. B* **1997**, *101*, 10560.

(26) Scholes, G. D.; Jordanides, X. J.; Fleming, G. R. *J. Phys. Chem. B* **2001**, *105*, 1640.

(27) Sumi, H. *J. Phys. Chem. B* **1999**, *103*, 252.

(28) Jang, S.; Newton, M. D.; Silbey, R. J. *Phys. Rev. Lett.* **2004**, *92*, 218301.

(29) Engel, G. S.; Calhoun, T. R.; Read, E. L.; Ahn, T.-K.; Mancal, T.; Cheng, Y.-C.; Blankenship, R. E.; Fleming, G. R. *Nature* **2007**, *446*, 782.

(30) Lee, H.; Cheng, Y.-C.; Fleming, G. R. *Science* **2007**, *316*, 1462.

(31) Iozzi, M. F.; Mennucci, B.; Tomasi, J.; Cammi, R. *J. Chem. Phys.* **2004**, *120*, 7029.

(32) Madjet, M. E.; Abdurahman, A.; Renger, T. *J. Phys. Chem. B* **2006**, *110*, 17268.

(33) Muñoz-Losa, A.; Curutchet, C.; Fdez. Galván, I.; Mennucci, B. *J. Chem. Phys.* **2008**, *129*, 034104.

(34) Curutchet, C.; Mennucci, B. *J. Am. Chem. Soc.* **2005**, *127*, 16733.

(35) Tomasi, J.; Mennucci, B.; Cammi, R. *Chem. Rev.* **2005**, *105*, 2999.

(36) Cohen, B. E.; McAnaney, T. B.; Park, E. S.; Jan, Y. N.; Boxer, S. G.; Jan, L. Y. *Science* **2002**, *296*, 1700.

(37) Golosov, A. A.; Karplus, M. *J. Phys. Chem. B* **2007**, *111*, 1482.

(38) King, G.; Lee, F. S.; Warshel, A. *J. Chem. Phys.* **1991**, *95*, 4366.

(39) Smith, P. E.; Brunne, R. M.; Mark, A. E.; Van Gunsteren, W. F. *J. Phys. Chem.* **1993**, *97*, 2009.

(40) Pitera, J. W.; Falta, M.; van Gunsteren, W. F. *Biophys. J.* **2001**, *80*, 2546.

(41) Simonson, T.; Brooks, C. L. *J. Am. Chem. Soc.* **1996**, *118*, 8452.

(42) Fidder, H.; Knoester, J.; Wiersma, D. A. *J. Chem. Phys.* **1991**, *95*, 7880.

(43) Scholes, G. D.; Fleming, G. R. *J. Phys. Chem. B* **2000**, *104*, 1854.

(44) Thompson, M. A.; Schenter, G. K. *J. Phys. Chem.* **1995**, *99*, 6374.

(45) Osted, A.; Kongsted, J.; Mikkelsen, K. V.; Astrand, P.-O.; Christiansen, O. *J. Chem. Phys.* **2006**, *124*, 124503.

(46) Nielsen, C. B.; Christiansen, O.; Mikkelsen, K. V.; Kongsted, J. *J. Chem. Phys.* **2007**, *126*, 154112.

(47) Öhrn, A.; Karlström, G. *Mol. Phys.* **2006**, *104*, 3087.

(48) Lin, Y.-l.; Gao, J. *J. Chem. Theory Comput.* **2007**, *3*, 1484.

(49) Muñoz-Losa, A.; Fdez. Galván, I.; Aguilar, M. A.; Martín, M. E. *J. Phys. Chem. B* **2007**, *111*, 9864.

(50) Casida, M. E. *In Recent Advances in Density Functional Methods*; Chong, D. P., Ed.; World Scientific: Singapore, 1995; Part I.

(51) Cammi, R.; Mennucci, B. *J. Chem. Phys.* **1999**, *110*, 9877.

(52) Hsu, C.-P.; Fleming, G. R.; Head-Gordon, M.; Head-Gordon, T. *J. Chem. Phys.* **2001**, *114*, 3065.

(53) Tretiak, S.; Middleton, C.; Chernyak, V.; Mukamel, S. *J. Phys. Chem. B* **2000**, *104*, 4519.

(54) Caldwell, J. W.; Kollman, P. A. *J. Phys. Chem.* **1995**, *99*, 6208.

(55) Case, D. A.; Darden, T. A.; Cheatham, T. E., III.; Simmerling, C. L.; Wang, J.; Duke, R. E.; Luo, R.; Merz, K. M.; Pearlman, D. A.; Crowley, M.; Walker, R. C.; Zhang, W.; Wang, B.; Hayik, S.; Roitberg, A.; Seabra, G.; Wong, K. F.; Paesani, F.; Wu, X.; Brozell, S.; Tsui, V.; Gohlke, H.; Yang, L.; Tan, C.; Mongan, J.; Hornak, V.; Cui, G.; Beroza, P.; Mathews, D. H.; Schafmeister, C.; Ross, W. S.; Kollman, P. A. *AMBER 9*, 9th ed.; University of California: San Francisco, 2006.

(56) Andersen, H. C. *J. Chem. Phys.* **1980**, *72*, 2384.

(57) Darden, T.; York, D.; Pedersen, L. *J. Chem. Phys.* **1993**, *98*, 10089.

(58) Ponder, J. W.; Case, D. A.; Valerie, D. *Adv. Protein Chem.* **2003**, *66*, 27.

(59) Gagliardi, L.; Lindh, R.; Karlström, G. *J. Chem. Phys.* **2004**, *121*, 4494.

(60) Karlström, G.; Lindh, R.; Malmqvist, P.-Å.; Roos, B. O.; Ryde, U.; Veryazov, V.; Widmark, P.-O.; Cossi, M.; Schimmelpfennig, B.; Neograd y, P.; Seijo, L. *Comput. Mater. Sci.* **2003**, *28*, 222.

(61) Frisch, M. J.; Trucks, G. W.; Schlegel, H. B.; Scuseria, G. E.; Robb, M. A.; Cheeseman, J. R.; Montgomery, J. A., Jr.; Vreven, T.; Kudin, K. N.; BurantJ. C., Millam, J. M.; Iyengar, S. S.; Tomasi, J.; Barone, V.; Mennucci, B.; Cossi, M.; Scalmani, G.; Rega, N.; Petersson, G. A.; Nakatsuji, H.; Hada, M.; Ehara, M.; Toyota, K.; Fukuda, R.; Hasegawa, J.; Ishida, M.; Nakajima, T.; Honda, Y.; Kitao, O.; Nakai, H.; Klene, M.; Li, X.; Knox, J. E.; Hratchian, H. P.; Cross, J. B.; Bakken, V.; Adamo, C.; Jaramillo, J.; Gomperts, R.; Stratmann, R. E.; Yazyev, O.; Austin, A. J.; Cammi, R.; Pomelli, C.; Ochterski, J. W.; Ayala, P. Y.; Morokuma, K.; Voth, G. A.; Salvador, P.; Dannenberg, J. J.; Zakrzewski, V. G.; Dapprich, S.; Daniels, A. D.; Strain, M. C.; Farkas, O.; Malick, D. K.; Rabuck, A. D.; Raghavachari, K.; Foresman, J. B.; Ortiz, J. V.; Cui, Q.; Baboul, A. G.; Clifford, S.; Cioslowski, J.; Stefanov, B. B.; Liu, G.; Liashenko, A.; Piskorz, P.; Komaromi, I.; Martin, R. L.; Fox, D. J.; Keith, T.; Al-Laham, M. A.; Peng, C. Y.; Nanayakkara, A.; Challacombe, M.; Gill, P. M. W.; Johnson, B.; Chen, W.; Wong, M. W.; Gonzalez, C.; Pople, J. A. *Gaussian 03, Revision C.02*; Gaussian, Inc.: Wallingford, CT, 2004.

(62) Rappe, A. K.; Casewit, C. J.; Colwell, K. S.; Goddard, W. A.; Skiff, W. M. *J. Am. Chem. Soc.* **1992**, *114*, 10024.

(63) Magyar, R. J.; Tretiak, S. *J. Chem. Theory Comput.* **2007**, *3*, 976.

(64) Müh, F.; Madjet, M. E.-A.; Adolphs, J.; Abdurahman, A.; Rabenstein, B.; Ishikita, H.; Knapp, E.-W.; Renger, T. *Proc. Natl. Acad. Sci. U.S.A.* **2007**, *104*, 16862.

CT9001366